RSC Advances




ROYAL SOCIETY OF CHEMISTRY

www.rsc.org/advances

# First-principles study of half-fluorinated silicene sheets

Xiao Wang,[a,*] Huangzhong Liu[b] and Shan-Tung Tu[c]

[a] School of Science, East China University of Science and Technology, Shanghai 200237, China

[b] Department of Equipment Economics Management, PLA Military Economics Academy, Wuhan 430035, China

[c] Key Laboratory of Pressure Systems and Safety, Ministry of Education, East China University of Science and Technology, Shanghai 200237, China

*Corresponding author. *E-mail address:* laricswang@gmail.com

Keywords

First-principles; Silicene; Fluorination; Electronic structures; Magnetism.

**Abstract**

The structural, electronic and magnetic properties of half-fluorinated silicene sheets are investigated using first-principles simulation. Three conformers of half-fluorinated silicene are studied and their properties are compared. Half-fluorinated silicene sheets with zigzag, boat-like or chair-like configurations are confirmed as dynamically stable based on phonon calculations. Upon the adsorption of fluorine, energy gaps open in both zigzag and boat-like conformations. They are found to be direct-gap semiconductors. The half-fluorinated silicene with chair-like configuration shows an antiferromagnetic behavior which is mainly induced by the un-fluorinated Si atoms. Furthermore, when isotropic strain is uniformly exerted onto chair-like half-fluorinated silicene, the energy difference between ferromagnetism states and antiferromagnetism states decreases with increasing compression strain from 0% to -6% or increasing tension strain from 0% to 6%. These results demonstrate that fluorination with different atomic configurations is an efficient way to tune the electronic structures and properties of silicene sheets and highlight the potential of half-fluorinated silicene for spintronics.

## 1. Introduction

Graphene, a two-dimensional (2D) honeycomb network of carbon atoms, has attracted lots of interests since Novoselov et al. first fabricated it in 2004.[1-3] It has zero-band-gap semi-metallic behavior with a Dirac-like electronic excitation and shows many remarkable properties such as high carrier mobility, quantum Hall effect for relatively low magnetic fields at room temperature and so on.[2,4] Because of these outstanding properties, graphene has been suggested to be a very promising candidate of the future electronic materials. To expand the applications of graphene-based materials into nanoelectronics and spintronics, fluorination is a promising and effective way to open the band gap and induce magnetism of it. Fluorine (F) atoms are introduced into graphene in the form of C-F covalent bond by $XeF_2$ fluorination.[5] Experimental and theoretical studies have indicated that the band gap of fluorinated graphene can be varied from 0 eV to about 3 eV with changing degrees of fluorination.[6-10] More interestingly, magnetism can be induced in half-fluorinated graphene which is an antiferromagnetic (AFM) semiconductor.[11]

The impressive progress in graphene has motivated the exploration of other 2D atomic based materials, such as BN and GaN sheet.[12,13] Researches on fluorinated BN and GaN sheets indicated that half-fluorinated BN sheet becomes a direct band gap semiconductor and is an antiferromagnet,[14] while half-fluorinated GaN shows ferromagnetism (FM) behavior.[11] As the counterpart of graphene, the 2D hexagonal lattices of silicon (Si), so-called silicene, recently were synthesized in the experiments.[15-21] Various studies have revealed that silicene not only has a similar electronic structure with graphene, but also has some unique features such as a large spin-orbit gap at the Dirac Point,[22] experimentally accessible quantum spin Hall effect,[23] electrically tunable band gap[24] and the emergence of a valley-polarized metal phase.[25] Because silicene sheets have recently been realized, it is highly desirable to investigate if fluorination of

silicene can induce some new effects. Ding et al.[26] have reported that after full fluorination, a direct band gap can be opened in the silicene fluoride and the gap values are continuously modulated by the strain. However, little work has been done to investigate the properties of partially fluorinated silicene, for example, the silicene with half of Si atoms saturated with F atoms. In addition, based on the previous studies, both silicene and full fluorinated silicene sheets are known to be nonmagnetic. Is it possible that half-fluorinated silicene can also be magnetic like half-fluorinated graphene? And does the arrangement of F atoms influence the properties of half-fluorinated silicene?

To explore these problems, in this work, we performed detailed first-principles calculations to investigate the structural, electronic and magnetic properties of the half-fluorinated silicene with three different conformers. On the basis of density functional theory (DFT) computations, it is found that the arrangement of the doped F atoms has significant influence on the electronic structures of silicene. Only half-fluorinated silicene with chair-like configuration shows magnetic behavior while zigzag and boat-like conformations become direct band-gap semiconductors with nonmagnetic. In addition, the strain effect on the magnetic properties of half-fluorinated silicene is also studied here.

## 2. Computational Methods

The present calculations have been performed by using the Castep package,[27] which is based on density functional theory (DFT). The exchange–correlation functional is treated within the generalized gradient approximation (GGA), in the form of Perdew–Burke–Ernzerhof (PBE) functional.[28] Ultrasoft pseudopotential[29] is adopted for the spin-polarized computation and the plane-wave cutoff energy is set to be 450 eV. In the pseudopotentials, the 3s, 3p shells of Si atom

and the 2s, 2p shells of F atom are treated as valence shells. Supercells are used to simulate the isolated nanostructures, and the distance between images is 20 Å to eliminate the interactions between the adjacent Si layers. The Brillouin zone is represented by the set of 10 x 10 x 1 k-points[30] for the geometry optimizations, and 15 x 15 x 1 k-points are used to obtain the density of states (DOS). All the lattice constants and atom coordinates are optimized until the convergence of the force on each atom is less than 0.01 eV/ Å. Also, the hybrid HSE03 functional[31] calculation by using norm-conserving pseudopotentials[32] is performed to obtain more correct description of band gaps due to the well-known problem of GGA calculations on evaluating the band gaps.

To determine the stability of the half-fluorinated silicene, the formation energy of the fluorinated single layer is estimated by calculating $E_f = (E_{total} - E_{pure} - N_F E_F)/N_F$, where $E_{total}$ is the energy of the half-fluorinated silicene, $E_{pure}$ is that of the pristine silicene, $E_F$ is the binding energy per atom of an $F_2$ molecule, and $N_F$ is the number of adsorbed F atoms.

## 3. Results and Discussion

### 3.1 Pristine silicene

The optimized geometric structure of pristine silicene is shown in Figure 1(a). The lattice parameter of relaxed silicene equals 3.866 Å and the Si−Si bond length is calculated to be d = 2.280 Å, consistent with previous results.[33,34] Compared with graphene, which has very strong π bonding and planar geometry, the larger Si−Si interatomic distance in silicene weakens the π−π overlaps and dehybridizes the $sp^2$ states which results in a low-buckled structure with h = 0.45 Å (Figure 1(b)). Silicene is also a semimetal (gapless semiconductor) like graphene[35,36] shown in Figure 2(a), in which a Dirac cone exists and is formed by the crossing of the bonding π and

antibonding π* bands at K points in the hexagonal Brillouin zone. In addition, the projected DOS (PDOS) in Figure 2(b) points out again that in silicene, the Dirac cone exists at the Fermi level and results from the $3p_z$ orbitals of Si atoms.

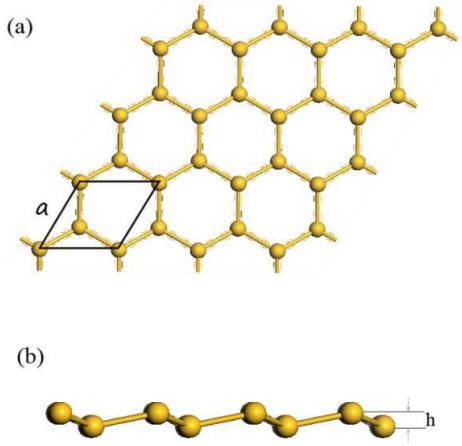


Figure 1. Optimized geometric structures of silicene from (a) the top view and (b) the side view. Silicon atoms are shown in yellow.

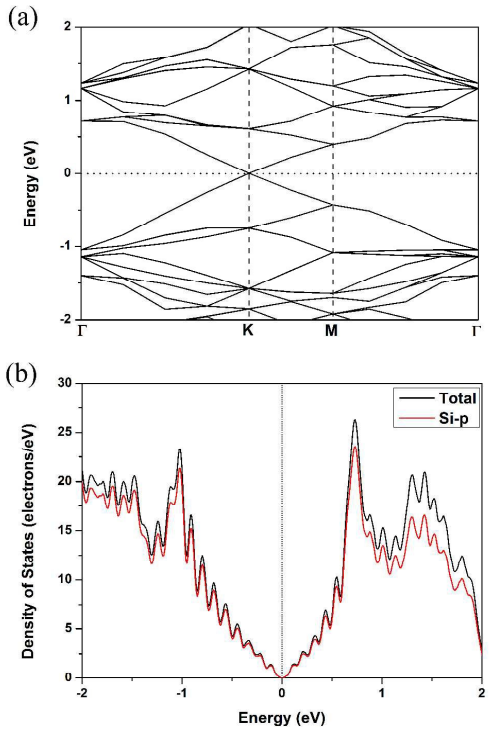


Figure 2. (a), Band structure of pristine silicene calculated after structural relaxation along high symmetry directions and (b) its PDOS. The Fermi level is set to 0 eV and displayed in dots.

### 3.2 Half-fluorinated silicene sheets

When silicene is exposed to gaseous fluorine, three possible atomic configurations of half-fluorinated silicene are considered: zigzag conformer with F atoms absorbed on the zigzag chains alternately (labeled as zigzag-F@$Si_2$ and shown in Figure 3(a)), boat-like conformer with F atoms distributed in pairs (labeled as boat-F@$Si_2$ and shown in Figure 3(b)), and chair-like conformer with F atoms doped alternately (labeled as chair-F@$Si_2$ and shown in Figure 3(c)). In these configurations, F atoms are only doped on one side of the silicene sheet. We defined $Si_1$ atoms as Si atoms remain unsaturated and $Si_2$ atoms as Si atoms doped by F atoms here. The optimized structural parameters and the formation energies of three conformers are listed in Table 1. Compared with pristine silicene, the bond lengths of Si-Si bonds in fluorinated silicene

have a varying degree of increase due to the formation of Si-F bonds. And the buckling heights $h_{buckle}$ of Si atoms increase significantly, especially for zigzag-F@$Si_2$ sheet. The formation energies of these half-fluorinated silicene are all negative, indicating that the fluorinations of silicene are exothermic reactions and the corresponding half-fluorinated silicene structures are stable. To verify the stability of half-fluorinated silicene, phonon calculations are also carried out and no imaginary frequencies are found in all the three conformers, indicating that the structures are dynamically stable. The phonon dispersion curves are plotted in Figure 4. The top frequencies are related with the Si-F bonds, which could be useful in characterizing these conformations. Among the three conformers, the zigzag configuration is the most stable one and the energies follow the order of $E_f$(zigzag) < $E_f$(boat-like) < $E_f$(chair-like) as shown in Table 1.

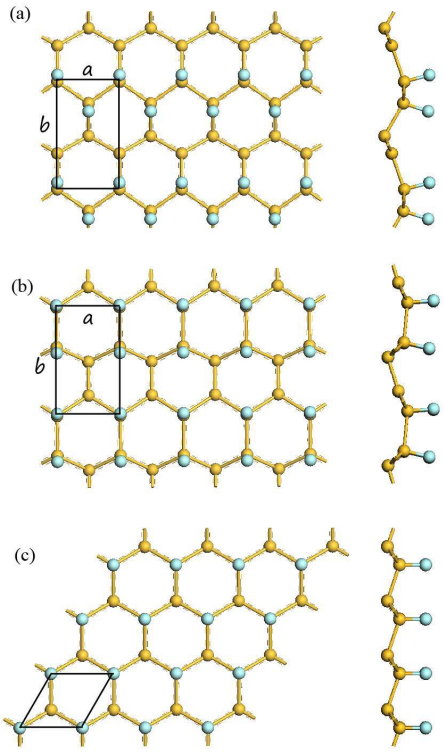


Figure 3. Top and side views of optimized structures of (a) zigzag, (b) boat-like, and (c) chair-like half-fluorinated silicene, respectively. Fluorine atoms are shown in blue.

Table 1. Lattice constants, bond lengths (in Å) and the formation energy (in eV/atom) of half-fluorinated silicene sheets. γ is the angle between the two lattice vectors.

| | Zigzag | Boat-like | Chair-like |
|---|---|---|---|
| *a* | 3.924 | 3.990 | 3.896 |
| *b* | 6.796 | 6.911 | - |
| γ | 90 | 90 | 60 |
| $h_{buckle}$ | 1.216 | 0.801 | 0.753 |
| $d_{Si1\text{-}Si1}$ | 2.296 | 2.231 | - |
| $d_{Si1\text{-}Si2}$ | 2.383 | 2.397 | 2.350 |
| $d_{Si2\text{-}Si2}$ | 2.391 | 2.448 | - |
| $d_{Si2\text{-}F}$ | 1.636 | 1.634 | 1.634 |
| $E_f$ | -3.575 | -3.519 | -3.311 |

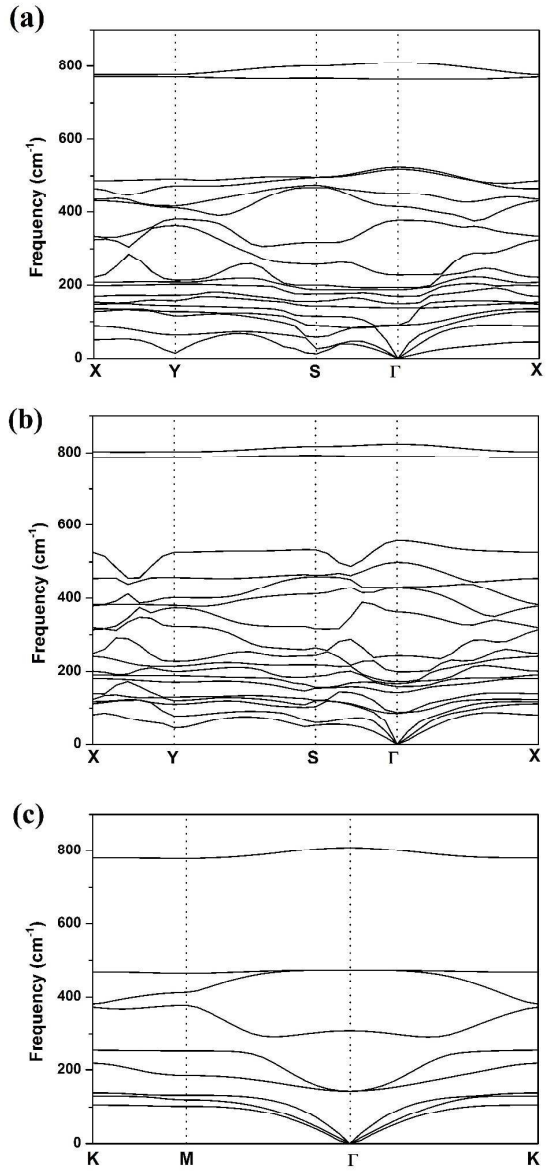


Figure 4. The phonon dispersion curves for three conformations of half-fluorinated silicene. (a) Zigzag; (b) boat-like and (c) chair-like.

In general, there are three kinds of Si-Si bonds existed in three conformations of half-fluorinated silicene: $Si_1$-$Si_1$, $Si_2$-$Si_2$ and $Si_1$-$Si_2$. To understand the charge transfer and bonding characters, we take the most stable conformer, zigzag half-fluorinated silicene sheet, as an example and present its electron density difference in Figure 5. The electron density difference

$\Delta\rho$ is defined as the difference between the total charge density of half-fluorinated silicene system and the superposition of independent charge density of silicene and F atoms.

$$\Delta\rho = \rho_{total} - (\rho_{silicene} + \sum\rho_{Fi})$$

where $\rho_{total}$, $\rho_{silicene}$ and $\rho_F$ denote electron density of zigzag half-fluorinated silicene sheet, pristine silicene and each F atoms, respectively. Loss of electrons is indicated in red, while electron enrichment is indicated in blue. When F atom doped on silicene sheet, a charge transfer from Si atom to F atom is clearly shown in Figure 5 which leaves Si atoms positively charged. The Si–Si bonds are strongly covalent while the Si–F bonds are primarily ionic mixed with partial covalent. Furthermore, it is worth noting that in Table 1 the $Si_1$–$Si_1$ bonds in zigzag-F@$Si_2$ and boat-F@$Si_2$ sheets are all shorter than the corresponding $Si_1$–$Si_2$ bonds and $Si_2$-$Si_2$ bonds. This is because that the $p_z$ orbitals on the $Si_2$ atoms are saturated by F atoms, which destroys the formation of $\pi$ bonding network in the $Si_1$–$Si_2$ bond and $Si_2$-$Si_2$ bonds, while besides the strong $\sigma$ bonds between the $Si_1$–$Si_1$ atoms, the $\pi$ bonds between the unpaired $p_z$ electrons of the $Si_1$ atoms are also formed, thus make the $Si_1$–$Si_1$ bond even shorter.

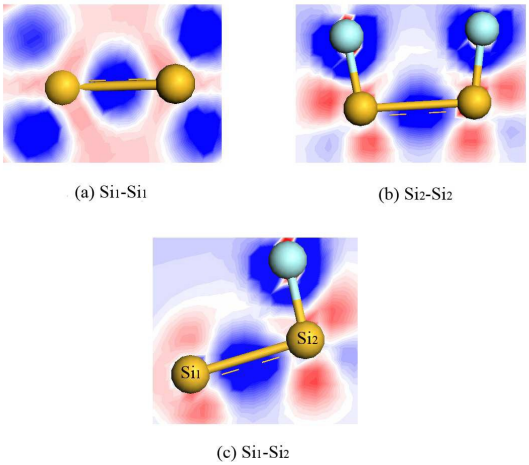


Figure 5. Electron density difference for three kinds of Si-Si bonds in zigzag-F@$Si_2$ sheet: (a), $Si_1$-$Si_1$ bond; (b), $Si_2$-$Si_2$ bond; (c), $Si_1$-$Si_2$ bond. Loss of electrons is indicated in red, while electron enrichment is indicated in blue.

The $sp^3$ hybridization of fluorine also affects the electronic structures of silicene. For the half-fluorinated silicene with zigzag and boat-like conformations, it is represented in Table 2 and Figure 6 that they become direct band-gap semiconductors, both the valence band maximum (VBM) and conduction band minimum (CBM) are located at the Γ point, and small gaps of 0.193 eV and 0.396 eV are opened, respectively. When Si atoms are exposed to F atoms, the $3p_z$ orbitals of Si atoms bond with 2p orbitals of F atoms, thus the weak coupling between Si atoms are broken which leads to the semiconducting nature of the systems. In Figure 7, the CBM of boat-F@$Si_2$ sheet is composed of the $p_z$ orbitals of unsaturated Si ($Si_1$) atoms and anti-bonding states of Si-F bonds, while the VBM is composed of the σ bonding states of $Si_1$-$Si_2$ bonds along the zigzag lines. When the half-fluorinated silicene has zigzag configuration, its VBM in Figures 8 is not only composed of the σ bonding states of $Si_1$-$Si_2$ bonds, but also the week π bonding between the unsaturated $Si_1$ atoms along the zigzag chain which makes a direct gap feature kept

but with a bit smaller gap of 0.193 eV compared with that of boat-F@$Si_2$ sheet. Additionally, to circumvent the problem of GGA calculations which usually underestimates the energy gap of semiconductors, the hybrid HSE03 calculations are performed to compare with the GGA results. The calculated energy gaps are also given in Table 2. For the systems studied here, the GGA energy gaps are found to be typically 40-55% smaller than the HSE results. However, there is no difference between the GGA and HSE evaluations on the type of the band gaps.

Table 2. Energy gaps of half-fluorinated silicene, computed by using GGA and HSE03 hybrid functionals.

| Conformers | Energy gap by GGA (eV) | Energy gap by HSE (eV) |
|---|---|---|
| Zigzag-F@$Si_2$ | 0.193 (direct) | 0.411 (direct) |
| Boat-F@$Si_2$ | 0.396 (direct) | 0.824 (direct) |
| Chair-F@$Si_2$ | 0.243 (direct) | 0.468 (direct) |

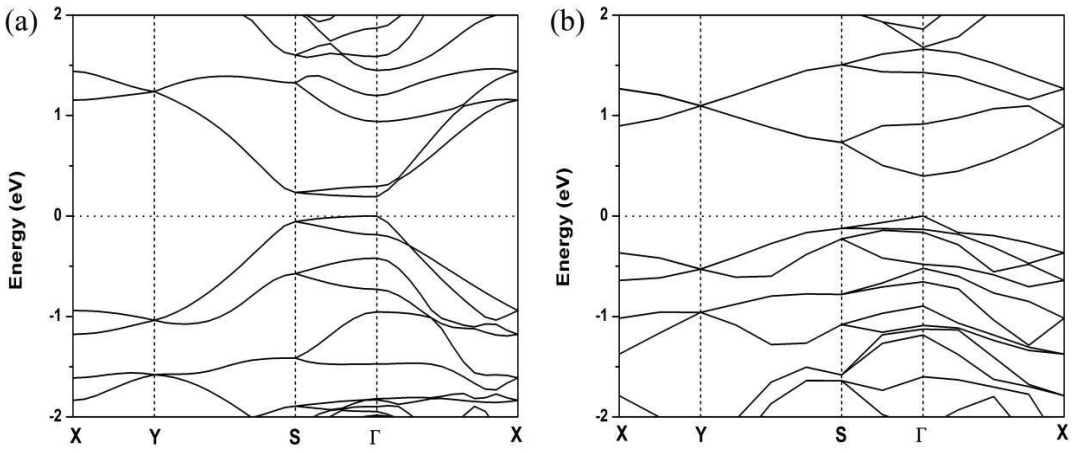


Figure 6. Band structures of (a) zigzag and (b) boat-like half-fluorinated silicene sheets, calculated using PBE functional. The Fermi levels are set as 0 eV and shown in dots.

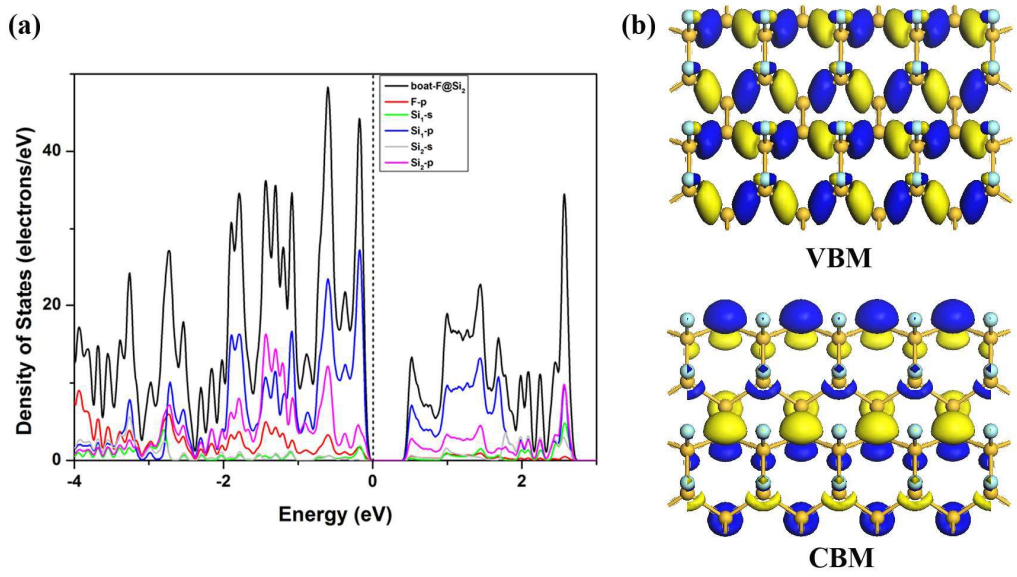


Figure 7. The PDOS (a) and (b) partial charge densities of VBM and CBM for the boat-like conformation of half-fluorinated silicene. The Fermi levels are set as 0 eV and shown in dots.

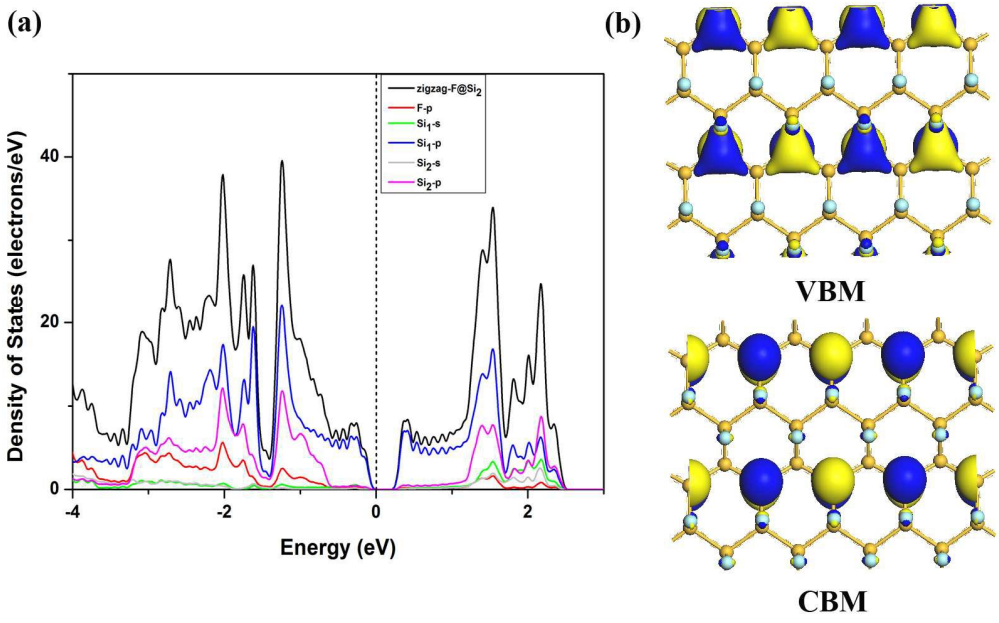


Figure 8. The PDOS (a) and (b) partial charge densities of VBM and CBM for the zigzag conformation of half-fluorinated silicene. The Fermi levels are set as 0 eV and shown in dots.

Although the boat-like and zigzag conformations of half-fluorinated silicene are nonmagnetic, Mulliken analysis shows that in the case of chair-F@$Si_2$ sheet, it is spin-polarized with a local magnetic moment of about 1$\mu_B$ per unit cell, similar with half-hydrogenated silicene or half-brominated silicene.[37,38] In order to study the preferred coupling, different magnetic configurations are presented in Figure 9: (1) nonmagnetic (NM); (2) FM coupling; (3) AFM coupling states within four types (A-AFM, G-AFM, H-AFM and P-AFM). Both PBE and HSE results are summarized in Table 3 and show that the A-AFM coupling is the most stable one and lies 0.104 and 0.406 eV (0.108 and 0.424 eV calculated by HSE) lower per unit cell in energy than that of FM and NM states, respectively, indicating that chair-F@$Si_2$ exhibits an AFM behavior. Also, the energies of G, H and P-type AFM states calculated by PBE functional are 0.009, 0.054 and 0.053 eV higher per unit cell than that of A-AFM coupling, respectively. Thus, the discussions in the following are focused on chair-F@$Si_2$ with A-AFM character and directly label it as AFM. The corresponding band structure of chair-F@$Si_2$ in AFM state is plotted in Figure 10, showing that the system is a direct semiconductor with band gap of 0.243 eV by GGA calculation. Detailed analysis of PDOS (Figure 11) reveals that the magnetism is mainly contributed by the unpaired 3p orbitals of unsaturated $Si_1$ atoms. In chair-F@$Si_2$ sheet, $Si_2$ atoms are bonded with F atoms forming strong σ-bonds; and the π-bonding network in the silicene sheet is broken, leaving $3p_z$ electrons of $Si_1$ atoms unpaired and localized. It is clearly shown in Figure 11 that spin splits near the Fermi level and thus induces magnetism. In fact, Mulliken population analysis shows that per $Si_1$ atom carried a magnetic moment of about 0.84 $\mu_B$, while very small magnetic moment was found on F and $Si_2$ atoms (about 0.02 and 0.01 $\mu_B$ per atom, respectively). The corresponding spatial spin-density distributions are illustrated in Figure 12.

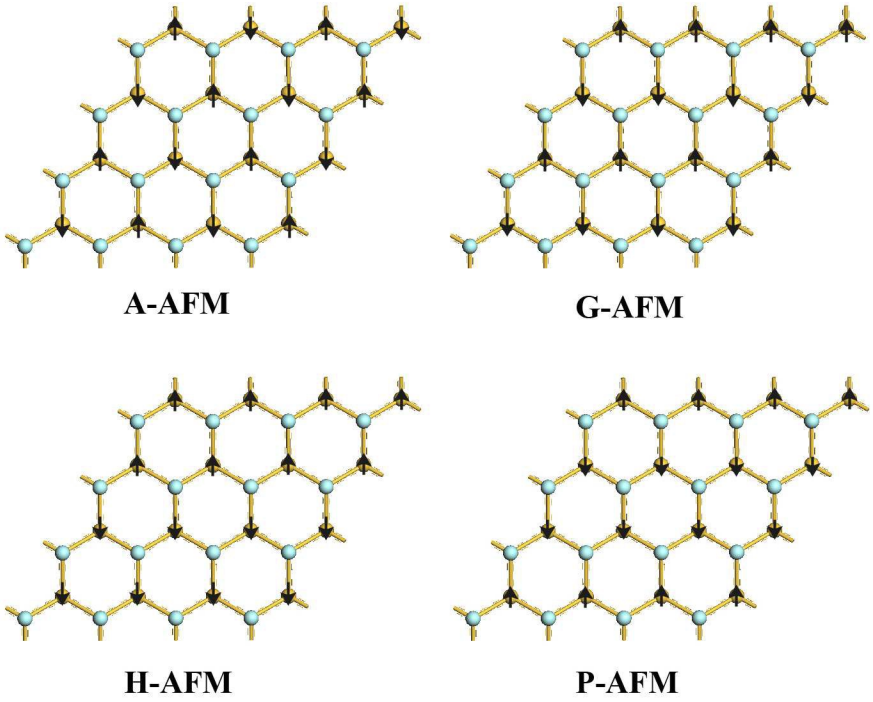


Figure 9. Different types of AFM coupling states of chair-F@$Si_2$ sheet.

Table 3. The relative energies per unit cell (in eV) and calculated magnetic moment (in $\mu_B$) for the atoms of chair-F@$Si_2$ in different magnetic configurations.

| Coupling | $\Delta E_{PBE}$ | $\Delta E_{HSE}$ | $M_{Si1}$ | $M_{Si2}$ | MF |
|---|---|---|---|---|---|
| NM | 0.406 | 0.424 | 0 | 0 | 0 |
| FM | 0.104 | 0.108 | 0.94 | 0.02 | 0.04 |
| A-AFM | 0 | 0 | ±0.84 | ±0.01 | ±0.02 |
| G-AFM | 0.009 | 0.002 | ±0.84 | ±0.01 | ±0.02 |
| H-AFM | 0.054 | 0.050 | ±0.90 | ±0.03 | ±0.06 |
| P-AFM | 0.053 | 0.053 | ±0.90 | ±0.02 | ±0.03 |

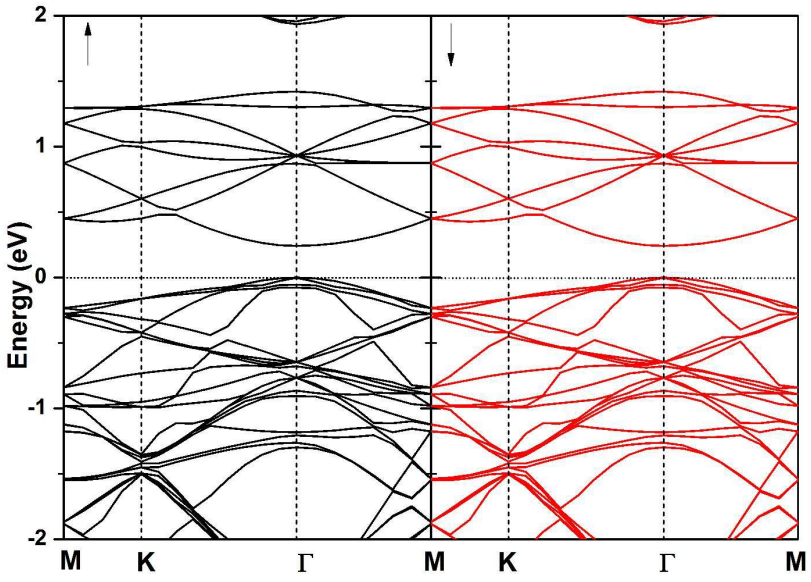


Figure 10. Band structure of chair-F@$Si_2$ sheet in A-AFM state, calculated using GGA functional. The arrows represent the spin direction.

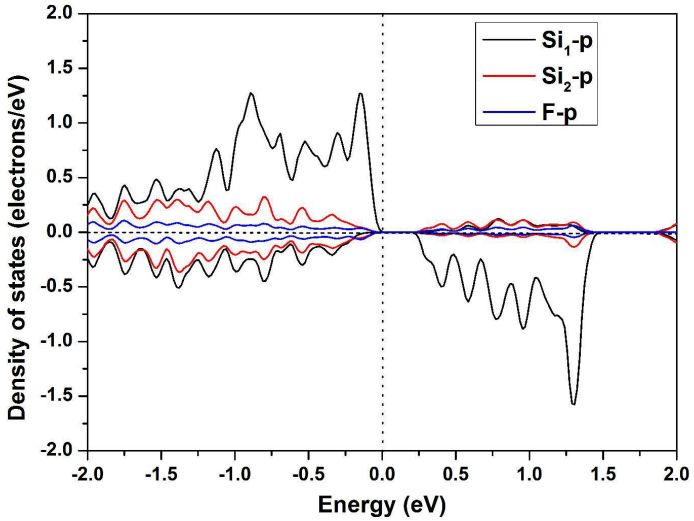


Figure 11. The PDOS of chair-F@$Si_2$ sheet in A-AFM state. The vertical dotted line represents the Fermi level.

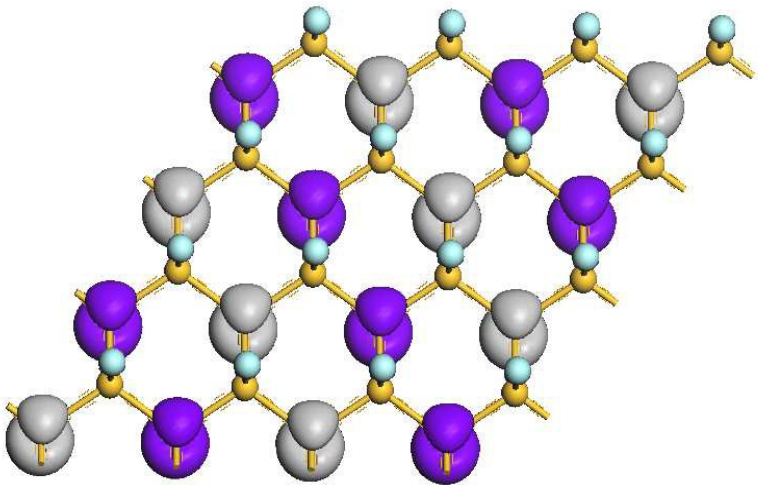

Figure 12. Spin density of chair-F@$Si_2$ sheet in A-AFM state. Purple and gray indicate the positive and negative values of spin, respectively.

### 3.3 Applied strain on chair-like half-fluorinated silicene sheet

Previous studies have indicated that the spin polarization exhibits remarkable radius dependence in F-BNNTs,[39,40] and increasing local tube curvature can enhance the relatively weak FM order in F-BNNTs. Another theoretical study on half-fluorinated BN sheet and graphene[11] showed that the energy difference between ferromagnetic and antiferromagnetic couplings decreases significantly with strain increasing. Motivated by these results, a nanomechanical modulation of strain may sensitively influence the spin order of half-fluorinated silicene. Thus, we investigate the strain dependence of spin order in chair-F@$Si_2$ sheet by varying the isotropic strain from -6% to 6%, in which all crystal symmetries and honeycomb-like structures are maintained. The in-plane tensile or compression strain is uniformly applied along lattice directions. The isotropic strain is defined as $\varepsilon = \Delta a/a_0$, where the lattice constants of the unstrained and strained supercell equal to $a_0$ and $a = \Delta a + a_0$, respectively. The stretching or compressing of the chair-F@$Si_2$ sheet is achieved by first elongating or shortening the optimized

lattice constant $a_0$ to a and re-optimized. Then the corresponding energy is calculated with the elongated or shortened lattice constant fixed. Figure 13 shows the variation in energy difference per unit cell between FM and AFM (A type) order ΔE of chair-F@$Si_2$ sheet with strain. Different with half-fluorinated graphene, it is found that for half-fluorinated silicene, ΔE dramatically decreases with increasing isotropic compression from 0% to -6% and also decreases gently with increasing isotropic tension from 0% to 6%. It indicates that the interaction between the moments keeps AFM coupling independent of the tension/compression, which reveals that the AFM spin order in chair-like half-fluorinated silicene is robust within a wide range of strain.

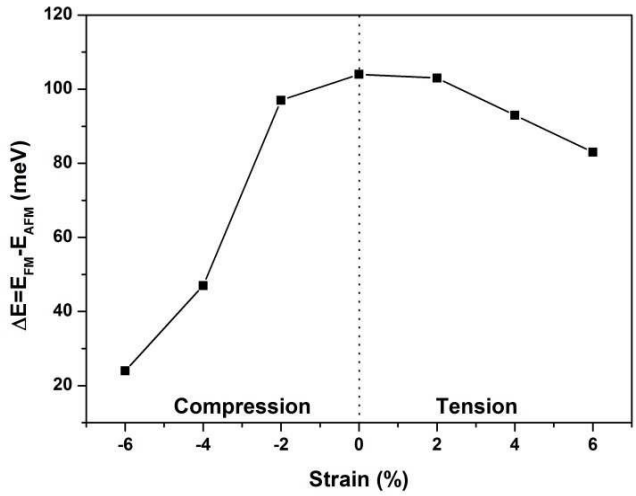


Figure 13. Strain dependence of the energy difference per unit cell between FM and AFM order of chair-F@$Si_2$ sheet.

According to the previous study by Ma et al.,[11] the magnetism of half-decorated 2D-sheets can be determined by the competition of two distinct interactions, through-bond interaction and p–p direct interaction. The through-bond interaction is defined as a kind of interactions that *a* atom with spin up (spin down) density induces a spin down (spin up) density on the adjacent *b*

atom which directly bonds to it. It is an indirect interaction mediated by *b* atom which may lead to FM spin coupling even in long range. In the situation of half-decorated silicene we studied here, *a* atom refers to unsaturated $Si_1$ atom and *b* atom means $Si_2$ atom doped by F atom. In contrast, the p–p direct spin polarization can induce the spin of the dangling bonds of *a* atoms into AFM coupling. In this kind of interaction, an *a* atom with spin up (spin down) density induces a spin down (spin up) density on the nearest-neighboring *a* atom directly, without mediated by *b* atom. In chair-F@$Si_2$ sheet, the strengthened bulking structure leads to the much larger spatial extension of 3p states of $Si_1$ atoms, which promotes direct p-p interaction and results in a more stable AFM coupling than the FM coupling. When strain is exerted on the sheet, the distance between two neighboring $Si_1$ atoms and the bond length of adjacent $Si_1$-$Si_2$ increases with increasing tensile strain (or decreasing compression strain), which results in the reduction of both through-bond and p–p direct interactions. The elongation of $Si_1$-$Si_2$ bond reduces bond energy and induces a little more spin-polarized electronic states (Figure 14). The magnetic moment $M_{Si1}$ of the strained chair-F@$Si_2$ sheet with $\varepsilon = 6\%$ slightly increases to 0.9 $\mu_B$. At the meantime, the decrease of the p-p interaction is a little larger than that of the through-bond interaction. As a result, for the chair-F@$Si_2$ sheet under tensile strain, the interaction between the moments keeps AFM coupling. On the other hand, PDOS of chair-F@$Si_2$ sheet under 6% compression demonstrates that the strengthened interaction between the adjacent Si atoms weakens the spin split of $Si_1$ 3p states, thus some unoccupied states sink below the Fermi level and become the occupied states. The magnetic moment $M_{Si1}$ is quenched from 0.84 $\mu_B$ to 0.38$\mu_B$, indicating that the magnetic coupling under such conditions is quenched. Although the AFM ordering is weakened for compression stress on chair-F@$Si_2$ sheet, however, the p–p interaction still plays a dominant role in spin polarization. As compared to the distance between two

neighboring $Si_1$ atoms, the bond length of $Si_1$-$Si_2$ decreases more obviously when the sheet is compressed. Thus, the increase of the through-bond interaction is larger than that of the p–p direct interaction with increasing compression strain, resulting in the relative decrease of the p–p direct interaction. This is why the energy difference ΔE decreases with increasing isotropic compression from 0% to -6%, also decreases with increasing isotropic strain from 0% to 6%. The variation of spin polarization in half-fluorinated silicene under strain may find applications in nanodevices, such as a mechanical switch for spin-polarized transport or many bistable devices.

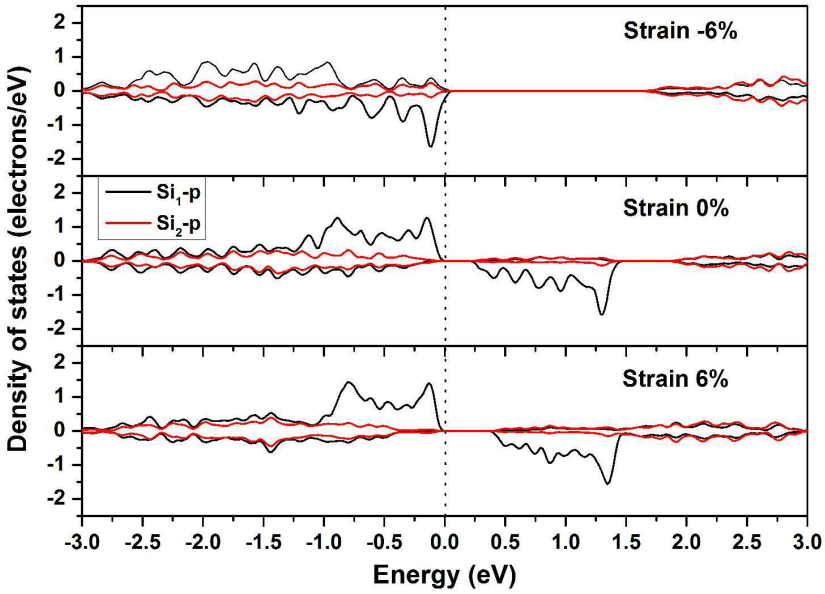


Figure 14. PDOS of chair-F@$Si_2$ under -6%, 0% and 6% strain, respectively. The vertical dotted line represents the Fermi level.

## 4. Conclusions

In conclusion, using first-principles calculations, we systematically investigate the structures and properties of half-fluorinated silicene. The atomic configurations have great effect on their electronic structures and magnetism. The zigzag conformer is also the most stable configuration of half-fluorinated silicene, same to the situation of full fluorination of silicene. And direct band gaps are opened in the zigzag-F@$Si_2$ and boat-F@$Si_2$ sheets with values of 0.411 and 0.824 eV obtained from the HSE03 functional, respectively. Only the half-fluorinated silicene with chair-like configuration shows antiferromagnetism. In chair-F@$Si_2$ sheet, electrons in $Si_1$ atoms are unpaired and localized, this results in spin polarization. Furthermore, the in-plane strain can be used to tune the relative stability of FM and AFM states of chair-F@$Si_2$ sheet due to the combined effects of both through bond and p–p direct interaction. Once combined with advanced Si nanotechnology, these predicted properties may be useful as a promising nanoscale technological application in electron component and spintronics.

**Acknowledgements**

The authors gratefully acknowledge financial support from NSFC (No. 21303054) and China Postdoctoral Science Foundation (2013M540332). All the computation simulation was undertaken with the resources provided from the High Performance Computing Center of East China University of Science and Technology.

**References**

1 A. K. Geim and K. S. Novoselov. *Nat. Mater.* 2007, **6**, 183.

2 A. H. Castro Neto, F. Guinea, N. M. R. Peres, K. S. Novoselov and A. K. Geim. *Rev. Mod. Phys*. 2009, **81**, 109.

3 K. S. Novoselov, A. K. Geim, S. V. Morozov, D. Jiang, Y. Zhang, S. V. Dubonos, I. V. Grigorieva, and A. A. Firsov. *Science* 2004, **306**, 666.

4 D. S. L. Abergel, V. Apalkov, J. Berashevich, K. Ziegler and T. Chakraborty. *Adv. Phys.* 2010, **59**, 261.

5 R. R. Nair, W. Ren, R. Jalil, I. Riaz, V. G. Kravets, L. Britnell, P. Blake, F. Schedin, A. S. Mayorov, S. J. Yuan, M. I. Katsnelson, H. M. Cheng, W. Strupinski, L. G. Bulusheva, A. V. Okotrub, I. V. Grigorieva, A. N. Grigorenko, K. S. Novoselov and A. K. Geim. *Small* 2010, **6**, 2877.

6 J. T. Robinson, J. S. Burgess, C. E. Junkermeier, S. C. Badescu, T. L. Reinecke, F. K. Perkins, M. K. Zalalutdniov, J. W. Baldwin, J. C. Culbertson, P. E. Sheehan and E. S. Snow. *Nano Lett.* 2010, **10**, 3001.

7 D. K. Samarakoon, Z. Chen, C. Nicolas and X. Q. Wang. *Small* 2011, **7**, 965.

8 S. H. Cheng, K. Zou, F. Okino, H. R. Gutierrez, A. Gupta, N. Shen, P. C. Eklund, J. O. Sofo and J. Zhu. *Phys. Rev. B* 2010, **81**, 205435.

9 K. J. Jeon, Z. Lee, E. Pollak, L. Moreschini, A. Bostwick, C. M. Park, R. Mendelsberg, V. Radmilovic, R. Kostecki, T. J. Richardson and E. Rotenberg. *ACS Nano* 2011, **5**, 1042.

10 J. C. Garcia, De D. B. Lima, L. V. C. Assali and J. F. Justo. *J. Phys. Chem. C* 2011, **115**, 13242.

11 Y. D. Ma, Y. Dai, M. Guo, C. W. Niu, L. Yu and B. B. Huang. *Nanoscale* 2011, **3**, 2301-2306.

12 J. C. Meyer, A. Chuvilin, G. Algara-Siller, J. Biskupek and U. Kaiser. *Nano Lett.* 2009, **9**, 2683.

13 H. Şahin, S. Cahangirov, M. Topsakal, E. Bekaroglu, E. Akturk, R. T. Senger, and S. Ciraci, *Phys. Rev. B* 2009, **80**, 155453.

14 J. Zhou, Q. Wang, Q. Sun and P. Jena. *Phys. Rev. B* 2010, **81**, 085442.

15 B. Lalmi, H. Oughaddou, H. Enriquez, A. Kara, S. Vizzini, B. Ealet and B. Aufray. *Appl. Phys. Lett.* 2010, **97**, 223109.

16 B. J. Feng, Z. J. Ding, S. Meng, Y. G. Yao, X. Y. He, P. Cheng, L. Chen and K. H. Wu. *Nano Lett.* 2012, **12**, 3507.

17 P. Vogt, De P. Padova, C. Quaresima, J. Avila, E. Frantzeskakis, M. C. Asensio, A. Resta, B. Ealet and G. Le Lay. *Phys. Rev. Lett.* 2012, **108**, 155501.

18 C. L. Lin, R. Arafune, K. Kawahara, N. Tsukahara, E. Minamitani, Y. Kim, N. Takagi and M. Kawai. *Appl. Phys. Express* 2012, **5**, 045802.

19 H. Jamgotchian, Y. Colignon, N. Hamzaoui, B. Ealet, J. Y. Hoarau, B. Aufray and J. P. Biberian. *J. Phys.: Condens. Matter* 2012, **24**, 172001.

20 D. Chiappe, C. Grazianetti, G. Tallarida, M. Fanciulli and A. Molle. *Adv. Materials* 2012, **24**, 5088.

21 L. Meng, Y. L. Wang, L. Z. Zhang, S. X. Du, R. T. Wu, L. F. Li, Y. Zhang, G. Li, H. T. Zhou, W. A. Hofer and H. J. Gao. *Nano Lett.* 2013, **13**, 685.

22 C. C. Liu, H. Jiang and Y. Yao. *Phys. Rev. B.* 2011, **84**, 195430.

23 C. C. Liu, W. X. Feng and Y. G. Yao. *Phys. Rev. Lett.* 2011, **107**, 076802.

24 N. D. Drummond, V. Zólyomi and V. I. Fal' ko. *Phys. Rev. B.* 2012, **87**, 075423.

25 M. Ezawa. *Phys. Rev. Lett.* 2012, **109**, 055502.

26 Y. Ding and Y. L. Wang. *Appl. Phys. Lett.* 2012, **100**, 083102.

27 M. D. Segall, P. J. D. Lindan, M. J. Probert, C. J. Pickard, P. J. Hasnip, S. J. Clark and M. C. Payne. *J. Phys.: Condens. Matter* 2002, **14**, 2717.

28 J. P. Perdew, K. Burke and M. Ernzerhof. *Phys. Rev. Lett.* 1996, **77**, 3865.

29 D. Vanderbilt. *Phys. Rev. B* 1990, **41**, 7892.

30 H. J. Monkhorst and J. D. Pack. *Phys. Rev. B* 1976, **13**, 5188.

31 J. Heyd, G. E. Scuseria and M. Ernzerhof. *J. Chem. Phys.* 2003, **118**, 8207.

32 D. R. Hamann, M. Schluter and C. Chiang. *Phys. Rev. Lett.* 1979, **43**, 1494.

33 S. Lebègue and O. Eriksson. *Phys. Rev. B* 2009, **79**, 115409.

34 X. D. Li, J. T. Mullen, Z. H. Jin, K. M. Borysenko, M. B. Nardelli and W. K. Kim. *Phys. Rev. B* 2013, **87**, 115418.

35 Y. C. Cheng, Z. Y. Zhu and U. Schwingenschlögl. *Euro. Phys. Lett.* 2011, **95**, 17005.

36 S. Cahangirov, M. Topsakal, E. Aktürk, H. Sahin and S. Ciraci. *Phys. Rev. Lett.* 2009, **102**, 236804.

37 C. W. Zhang and S. S. Yan. *J. Phys. Chem. C* 2012, **116**, 4163.

38 F. B. Zheng and C. W. Zhang. *Nanoscale Res. Lett.* 2012, **7**, 422.

39 Z. H. Zhang and W. L. Guo. *J. Am. Chem. Soc.* 2009, **131**, 6874.

40 F. Li, Z. Zhu, X. Yao and G. Lu. *Appl. Phys. Lett.* 2008, **92**, 102515.

**Table of Contents**

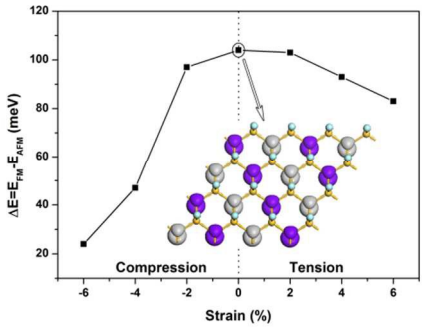


Strain dependence of the energy difference between FM and AFM order of chair-F@$Si_2$ sheet. Inserted image shows the spin density distribution of chair-F@$Si_2$ sheet with no strain.